Supersonic Inflatable Aerodynamic Decelerators for use on Sounding Rocket Payloads

Matthew J. Miller,[1] Bradley A. Steinfeldt,[2] Robert D. Braun[3]
Georgia Institute of Technology, Atlanta, GA, 30332

This paper presents an assessment of a supersonic inflatable aerodynamic decelerator for use on a sounding rocket payload bus structure for a high-altitude sample return mission. Three decelerator configurations, the tension cone, attached isotensoid, and the trailing isotensoid, were examined on the metrics of decelerator mass, aerodynamic performance, and vehicle integration. The attached isotensoid configuration is shown to be the least mass solution. Aerodynamic analysis shows that a drag performance degradation of up to 40% for the attached decelerators results when the attachment point is recessed from the forebody of the bus structure. Vehicle integration mechanisms are identified and examined for each decelerator configuration. Using multiattribute decision making techniques, the trailing isotensoid is identified to be the most advantageous decelerator option for use in this application.

Nomenclature

A	= area, m^2
C_D	= coefficient of drag
$C_D A$	= drag area, m^2
d_f	= areal density, kg/m^2
ε_t	= ratio of minor torus diameter to overall diameter
M	= Mach number
q_{deploy}	= deployment dynamic pressure, Pa
ρ	= atmospheric density, kg/m^3
T_0	= stagnation temperature, K

I. Introduction

Small payload bus technology is allowing access to space to become more affordable. Initiatives such as the NASA Cubesat Launch Initiative and the NASA Sounding Rocket Program are growing programs for the small satellite community.[1,2] Private companies as well as universities are producing tightly packaged payloads that can be launched as secondary payloads on orbital launch and suborbital sounding rocket vehicles to conduct space technology demonstrations and science. More specifically, there is a growing interest in upper atmospheric interstellar dust and how it influences noctiluent cloud formation.[3] Sounding rocket campaigns have primarily focused on *in situ* measurements of these interstellar particles with extremely limited sample return capability.[4,5,6,7] This study proposes enhancement of payload return capability can be made by utilizing a supersonic inflatable aerodynamic decelerator, IAD.

First proposed in the 1960's, IADs are mass efficient devices capable of increasing a vehicle's drag area. Compared to conventional parachute technology, IADs are capable of being deployed at higher dynamic pressures and Mach numbers enabling additional deceleration.[8] Numerous flight tests were conducted until the mid-1970's which examined the aerodynamic drag performance and stability of IADs.[9,10] A typical use for an IAD is to increase the landed mass of an entry vehicle on a planetary body.[11] However, the purpose of the IAD in this investigation is to perform as a range control device. This study builds upon previous work found in Ref. [3] by examining three inflatable aerodynamic decelerators: a tension cone, attached isotensoid, and trailing isotensoid considering mass, aerodynamic performance, and vehicle integration.

---

[1] Graduate Research Assistant, Guggenheim School of Aerospace Engineering, mmiller@gatech.edu, AIAA Student Member
[2] Research Engineer II, Guggenheim School of Aerospace Engineering, bsteinfeldt@gatech.edu, AIAA Member
[3] David and Andrew Lewis Associate Professor of Space Technology, Guggenheim School of Aerospace Engineering,
  robert.braun@aerospace.gatech.edu, AIAA Fellow

II.   Mission Architecture

A. Trajectory & Deployment Definition

As discussed in previous work,[12,13] drag modulation is a guidance technique used to control downrange travel by adjustment of a vehicle's drag area. The vehicle drag area for this investigation is modified by the inflation of a decelerator device. The baseline trajectory, optimized for maximum time in the mesosphere, from Ref. [3] was leveraged to establish a reference trajectory for this analysis. The reference trajectory of an Improved-Orion sounding rocket launched at a flight path angle of 81 degrees with a 24 kg payload is shown in Figure 1. The trajectory shown in Figure 1 does not include any deployment events and terminates at an altitude of 6 km. The terminal state corresponds to the nominal deployment altitude of a guided parafoil, which is not discussed in this study. The nominal trajectory provides 184 seconds of sample collection time within the mesosphere. Nominal decelerator deployment occurs after the sample collection phase at an altitude of 45 km at Mach 2.9 and a dynamic pressure of 1 kPa. Within a prescribed deployment box between the altitudes of 25 km and 45 km, peak Mach number and dynamic pressure values were 3 and 6 kPa, respectively.
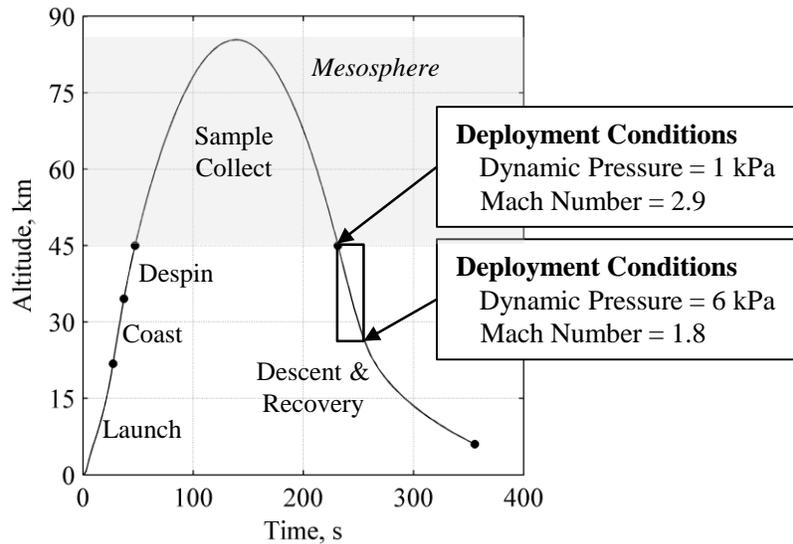

Figure 1. Baseline trajectory altitude as a function of time.

Decelerator deployment conditions for this study, assumed to be a conservative Mach 3 and dynamic pressure of 2 kPa, were compared to historical testing and are summarized in Figure 2. Deployment conditions are similar to the ALARR testing conducted in the 1960's for trailing decelerators.
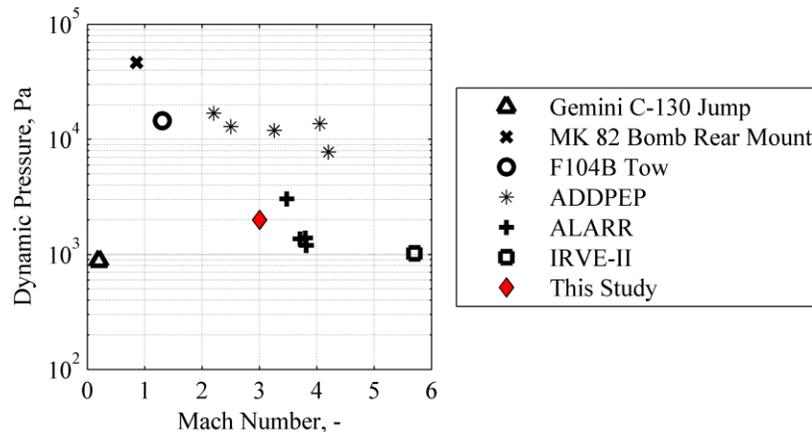

Figure 2. Inflatable decelerator deployment conditions (dynamic pressure and Mach number) of historical test programs and the conditions proposed in this study. (Data reproduced from Figure 2 in Ref. [8])

1

B. Sounding Rocket Configuration

The Improved-Orion provides the launch capability necessary to reach the mesosphere. The outer mold line of the Improved-Orion is shown in Figure 3. This vehicle can accommodate a variety of payload diameters, 4.5 to 17 inches, with its bulbous fairing option, which is also shown in Figure 3.[2]
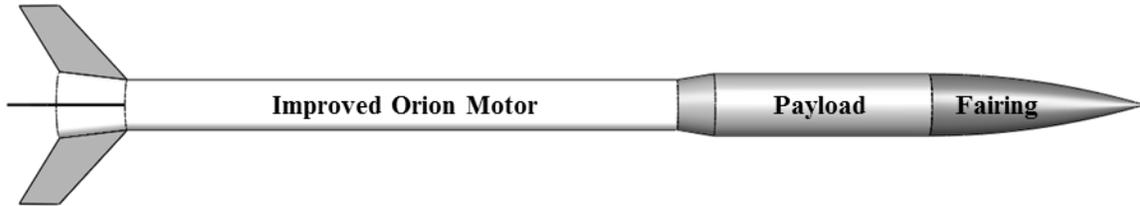

Figure 3. Improved Orion sounding rocket with bulbous payload fairing.

1. Payload Bus & Sample Collection Device

Typical payload configurations for the launch vehicles under consideration utilize a cylinder with a diameter of 0.356 m and a length of 1.22 m as shown in Figure 4. The sample collection mechanism was assumed to be a container fitted with Aerogel pucks. Aerogel was proven as a viable medium for capturing high velocity particles in outer space on the Stardust mission[14] and could be implemented for sounding rocket particle capturing. The detailed design of the sample collection device is outside the scope of this study; however, it is assumed that the Aerogel would be exposed to the freestream during the sample collection phase without altering the vehicle aerodynamics. After sample collection, the containment device would seal the Aerogel pucks, preventing the samples from being contaminated during recovery.
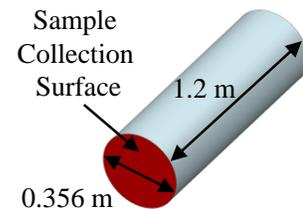

Figure 4. Representative cylindrical bus structure.

C. Decelerator Configurations

1. Tension Cone

The tension cone consists of two primary fabric components: a flexible shell that resists shape deformation by remaining under tension and an inflated torus. The curvature is analytically derived based on a pressure distribution and assumed constant ratio of circumferential to meridional stress. The shell of the tension cone is attached to the forebody at the front of the vehicle and to an inflated torus. An onboard inflation system is required to inflate the torus and to maintain the internal pressure of the torus. The baseline tension cone, scaled from wind tunnel test articles[15,16] had an overall diameter of 0.9 m with a torus diameter of 0.1125 m as shown in Figure 5. A detailed description of tension cone IADs can be found in Ref. [17].These images provide a sense of scale between the sounding rocket bus and tension cone.
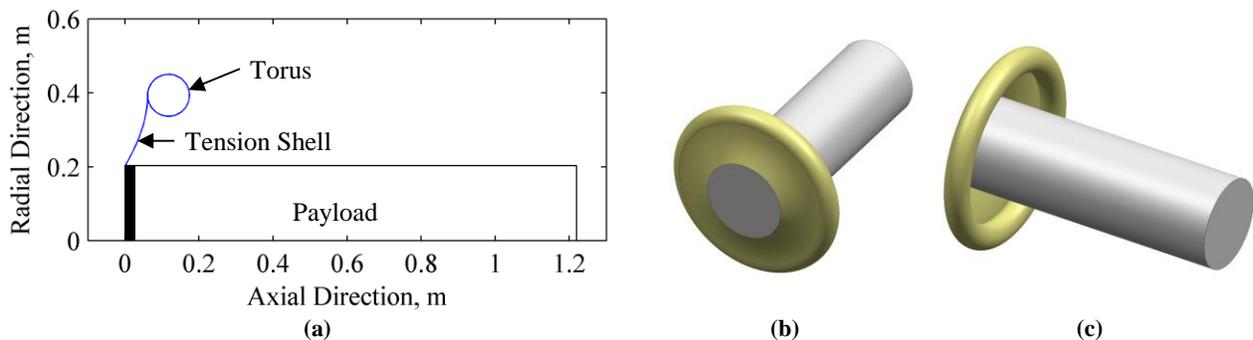

(a)   (b)   (c)

Figure 5. Tension cone (a) dimensions, (b) frontward isometric, and (c) rearward isometric integrated with payload bus structure.

2

2. Attached Isotensoid

The isotensoid configuration is examined as an attached and trailing configuration. The decelerator itself is largely the same for each configuration, except for how the decelerator is integrated with the bus structure. The isotensoid shape enables constant tension throughout the length of the meridians and a uniform biaxial stress across the gore fabric. Ram air inlets, not shown in Figure 6, maintain internal pressure of the device, thus no onboard inflation system is required to maintain the inflated shape. However, a pre-inflation system is typically needed to subject the ram air inlets to the freestream for inflation to start. The attached isotensoid shape used in this study was derived from the work conducted by Barton in Ref. [18] and had an overall diameter of 0.99 meters which includes the burble fence. A detailed description of the isotensoid can be found in Refs. [18] [15].
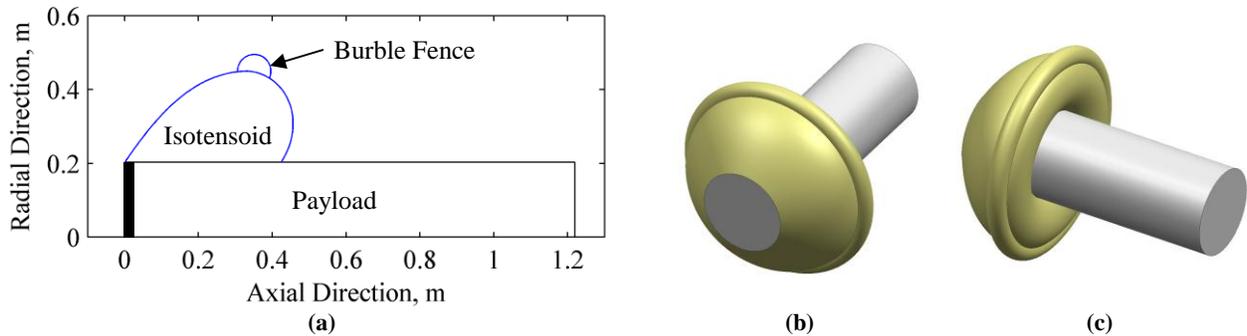

Figure 6. Attached isotensoid (a) dimensions, (b) frontward isometric, and (c) rearward isometric integrated with payload bus structure.

3. Trailing Isotensoid

The trailing isotensoid is deployed by an ejection event and trails behind the vehicle's bus. The decelerator inflates in a similar manner as the attached isotensoid, except the device is located at some predefined trailing length behind the bus. The representative trailing isotensoid for this study, as shown in Figure 7, was taken from Ref. [19].
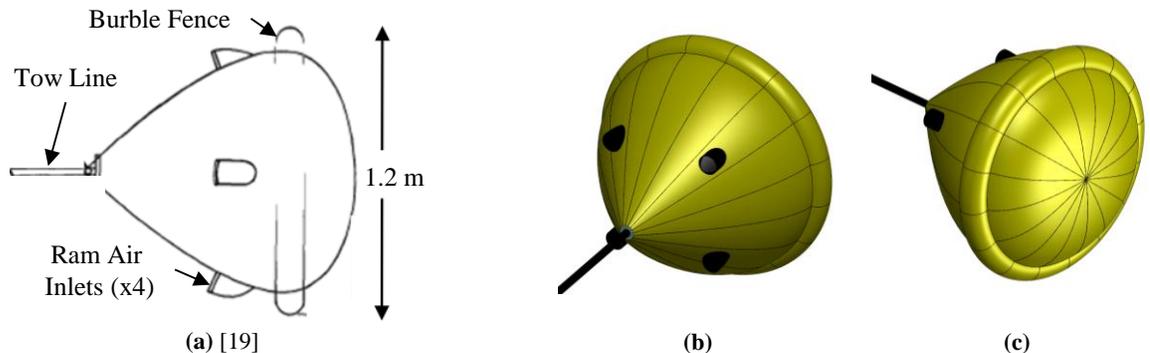

Figure 7. Trailing isotensoid (a) dimensions, (b) frontward isometric, and (c) rearward isometric integrated with payload bus structure.

III. Design Metrics

A. Aerodynamics

Two aerodynamics analyses were implemented to characterize the aerodynamic performance of the tension cone and attached isotensoid aerodynamic decelerators—a hypersonic panel method with engineering correlations to the supersonic regime, CBAERO, [20] and a computational fluid dynamics (CFD) package, FUN3D. Trailing isotensoid aerodynamic performance was obtained from heritage wind tunnel and in-flight experimentation. Calculation of the interactions of blunt body wakes on trailing decelerators is outside of the scope of this study. Therefore, the heritage sources were leveraged for the trailing decelerator. All aerodynamic performance values were generated at zero angle-of-attacks relative to the free stream.

1. Computational Fluid Dynamics Method

The CFD simulation was performed in FUN3D, which is a fully unstructured, 3-dimesional fluid solver with both Euler and Reynolds average Navier Stokes equation capabilities.[21,22] For this study, inviscid, calorically perfect, compressible equations were assumed with local time stepping. Grids were generated using Gridgen[23] and consist of between 0.8 and 0.9 million grid points. All CFD solutions were generated using the input variable values shown in Table I.

Table I. FUN3D parameters.

Variable	Value	Units
M	4.0	-
ρ	0.0577	kg/m^3
T_0	219	K
V	1,181	m/s

In addition to the nominal attachment point, the effect of attachment point locations on decelerator drag performance was also investigated. Figure 8 shows four alternative forward attachment point locations. The alternative attachment points were incremented by 5% of the length of the vehicle bus resulting in a maximum attachment point offset distance of 0.244 m from the front of the vehicle bus. These alternative attachment points were to account for the possibility of a more complicated sample collection device.
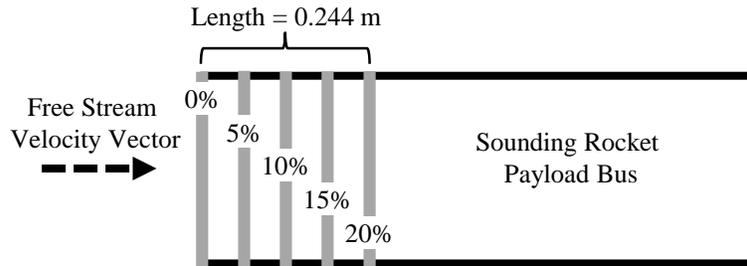

Figure 8. Decelerator front attachment point locations along the length of the vehicle bus.

B. Mass Estimation

To account for the mass addition of each decelerator system, mass estimates were obtained for all three aerodynamic decelerators based on parametric sizing techniques and historical regressions.

1. Tension Cone

The mass for the tension cone was determined using the dimensionless parameter technique developed by Samareh.[24] The total tension cone system's mass was calculated by the summation of eight different dimensionless elements: the inflation gas, the inflation systems mass, the toroid fiber mass, the toroid adhesive mass, the toroid gas barrier mass, the toroid axial straps mass, the radial straps mass, and the gore mass.

The tension cone input configuration for this study is summarized in Table II. All other input parameters used in Samareh's mass sizing technique were assumed to be the same as referenced in Ref. [24]. A 30% mass margin was added to all of the resulting mass for each the tension cone decelerator to account for any miscellaneous mass and uncertainty not accounted for in this analysis.

Table II. Tension cone input parameters.

Input Parameter	Value
Dynamic Pressure (Pa)	2000
Number of Toroid	1
Area Ratio	6.39
Radius Ratio	7
Diameter of Torus Circle (m)	0.1125
Diameter of Torus (m)	0.7875
ε_t (D_t/D_0)	0.1429
Vehicle Bus Diameter (m)	0.356
Tension Cone Drag Coefficient	1.5
Number of Radial Straps	16

2. Trailing Isotensoid

The trailing isotensoid mass was calculated using a relationship accounting for the structural and aerodynamic parameters which govern the decelerator efficiency.[25] Equation 1 shows this relation where the first term at accounts for the mass of meridian tapes and rise and suspension lines and the second term accounts for the canopy mass.

$$m_{Iso} = bq_{deploy}(C_D A)^{3/2} + cd_f(C_D A)$$

Eqn (1)

4

The aerodynamic drag area ($C_D A$) is of the trailing isotensoid only. The constants b and c, which were derived from pressure vessel theory, are specified by Anderson to be 6.9×10^{-5} kg/N-m and 7.41, respectively.[25] From the baseline trajectory, the dynamic pressure at deployment is 2 kPa and d_f is the areal density of the canopy fabric (kg/m^2). A 50% mass margin on the resulting mass for the trailing isotensoid to account for any miscellaneous mass and uncertainty not accounted for in this analysis.

The deployment mechanism for the trailing isotensoid requires a mortar similar to that of a typical parachute system.[17] The mortar mass required to eject a given trailing isotensoid was estimated from a linear regression of historical data for subsonic parachutes of similar masses, shown in Figure 9.

Figure 9. Mortar mass vs. parachute mass regression (Ref. [16])

3. Attached Isotensoid

The attached isotensoid mass was calculated using the relation as the trailing isotensoid described in Eqn. (1). However, the constants b and c were altered to 1.1×10^{-5} kg/N-m and 4.02, respectively, to account for the changed isotensoid configuration as suggested in Ref. [25]. As with the trailing isotensoid, a 50% mass margin was also included in the attached isotensoid mass estimate to account for uncertainty associated with this empirical mass estimation method.

4. Decelerator Material Properties

All decelerator masses were evaluated using a variety of materials detailed in Table III, where $\bar{\sigma}$ is a non-dimensional yield stress as described in Ref. [24].

Table III. Material properties for decelerator systems.

Material	Density (kg/m^3)	Areal Density (kg/m^2)	Tensile Strength (GPa)	$\bar{\sigma}$ (-)	Reference
Vectran	1,400	0.0916	1.10	80,093	[26] [27]
(Coated) Vectran	1,500	0.1457	3.20	217,465	[26] [27]
Kevlar 29	1,440	0.2080	2.92	206,705	[28] [29]
Kevlar 49	1,440	0.1810	3.00	212,368	[28] [29]
(Coated) Kevlar	1,500*	0.3750	3.00	203,874	[28] [29]
Upilex-25S	1,470	0.3778**	0.52	36,059	[30]
Nomex	1,380	0.4001	0.61	45,059	[31]
Nextel (610)	3,900	0.2780	3.20	83,640	[32] [17]

*Density estimated based on coated Vectran
**Upilex minimum gage areal density estimated based on 50 micrometer fabric thickness and scaled by same factor as Nomex

The materials used in this analysis encompass heritage materials such as Nomex and Nextel and more modern materials such as Vectran and Kevlar to capture the advancements that have been made in the material sciences field. Coated materials which reduce fabric porosity are also included in this study.[17] Areal density values are assumed to be minimum gage values with the exception of Upilex-25S and Nomex. The minimum gage areal density of Nomex is 0.078 kg/m^2; however, flight test articles from Ref. [33] deployed trailing decelerators at high dynamics pressures (11-17 kPa) made of Nomex with an areal density equal to 0.4 kg/m^2. The minimum gage areal density of Nomex was linearly scaled to match the test article areal density and the same scaling value was applied to Upilex-25S, since both materials share similar material properties.
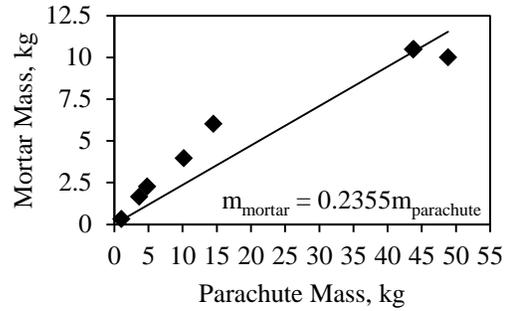
C. Vehicle Integration

To evaluate each mechanism in a qualitative manner, the analytical hierarchy process (AHP) was used.[34,35] AHP is a multi-attribute decision-making technique that uses pairwise comparisons. Prioritization of objectives is obtained from populating a matrix of pairwise comparisons. A vector of weights indicating the relative importance of each objective is then obtained. For this study, each mechanism served as an objective and were compared to each other using an objective scoring system which ranged from extremely prefer to neutral. The storage volume for each decelerator was also examined for each decelerator assuming a nominal parachute nonpressurized packaging density of 320 kg/m^3 for a range of decelerator drag areas.[36]

D. Decelerator Evaluation

AHP was utilized to determine a vector of preferential weights for each of the aforementioned design metrics. The priority vector for each design metric was then used in an additional analysis, the Technique for Order Preference by Similarity to Ideal Solution (TOPSIS). This method allows for scoring of alternatives based on their Euclidean distances from the positive ideal and negative ideal solutions.[35,37,38] The combination of the AHP priority vectors for each individual design metric and an overall design metric weighting vector enabled the use of TOPSIS to yield a final decelerator downselection option for this mission concept.

IV. Decelerator Results and Discussion

A. Aerodynamics Results

Historical testing programs have examined the drag performance of the three decelerators under investigation.[8,9,15] For this analysis, CBAERO results consistently over predicted the drag coefficient of the attached isotensoid and tension cone by approximately 13%. This consistent over prediction is attributed to CBAERO's inability to account for the drag coefficient of the front face of the cylinder. The pressure distribution on the cylinder's front face is greatly influenced by the bow shock which is not taken into account in the CBAERO panel method. The inviscid CFD solutions for both decelerators were in good agreement with historical drag coefficient values.

The aerodynamic performance of the trailing decelerator is difficult to predict due to the unsteady nature of the wake flowfield region behind the forebody bus structure. However, experimental testing showed trailing decelerators exhibit stabilizing characteristics for a variety of Mach number regimes and decelerator-to-payload size ratios.[9] Therefore, the drag coefficient values shown in the literature were directly used for the trailing isotensoid.

Aerodynamic performance of the tension cone and attached isotensoid were analyzed for a variety of attachment points, since the sample collection mechanism is not clearly defined at this stage in the design process. As the decelerator moves farther rearward, drag performance diminishes substantially as shown in Figure 10. The decelerator becomes shadowed by the oblique shock which forms from the corner of the bus forebody, thus reducing the decelerator's overall drag coefficient. The CFD Mach contour solutions to the 0% offset and 20% offset solutions for the baseline tension cone are shown in Figure 11. The bow shock changes for the varied attachment points, which results in altered pressure distributions on the surface of the decelerator. This altered pressure distribution leads to reduced drag performance for the offset attachment points. The altered bow shock also alters the pressure distribution on the bus forebody. The results from this analysis indicate that if drag performance is to be maximized for a fixed diameter decelerator, the attachment point must be at 0% offset. The alternative to this solution would be to increase the attachment offset but increase the diameter of the decelerator which would also increase the overall mass of the decelerator subsystem.
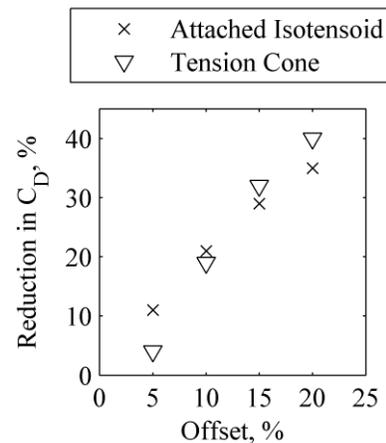

Figure 10. Drag coefficient reduction as a function of attachment offset.
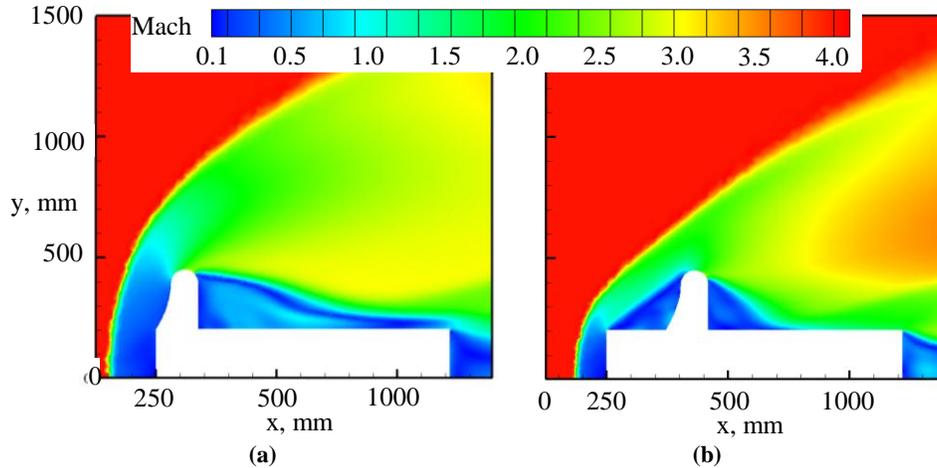
Figure 11. Mach contour plots of (a) 0% offset tension cone and (b) a 20% offset tension cone configuration.

Taking into account the aerodynamic drag coefficient values at a nominal deployment condition of Mach 3, a priority vector was created. As shown in Table IV, this aerodynamic priority vector was implemented in the overall TOPSIS analysis for decelerator evaluation. The larger number corresponds to the more favorable decelerator option, which was the tension cone.

Table IV. Aerodynamic AHP Results

Decelerator Type	Priority Vector
Tension Cone	0.448
Attached Isotensoid	0.383
Trailing Isotensoid	0.168

B. Mass Estimation Results

The mass estimates for the three types of decelerators are shown below for the eight decelerator materials considered in this study. These mass results are for each decelerator type being attached to a 0.356 m diameter cylindrical bus. Figure 12 shows the mass estimates for the tension cone. Tension cones which use higher strength materials such as Vectran or Kevlar, exhibit significantly less overall mass, especially at larger drag areas. Tension cones require an inflation system which increases the mass growth at an exponential rate due to its dependence on torus volume. Figure 13 shows the results for the attached isotensoid decelerator. Again, higher strength materials exhibit more mass efficient solutions. Figure 14 shows mass trends for the trailing isotensoid configuration which also follow almost linear mass growth rates. It is important to note that the mass calculations for the tension cone include estimates of inflation hardware, whereas the isotensoid calculations do not. The trailing isotensoid mass must be summed with a deployment system mass expected to be on the order of 1 kg, as shown in Figure 9. Attachment and storage mechanism are not included in any of these mass estimates.
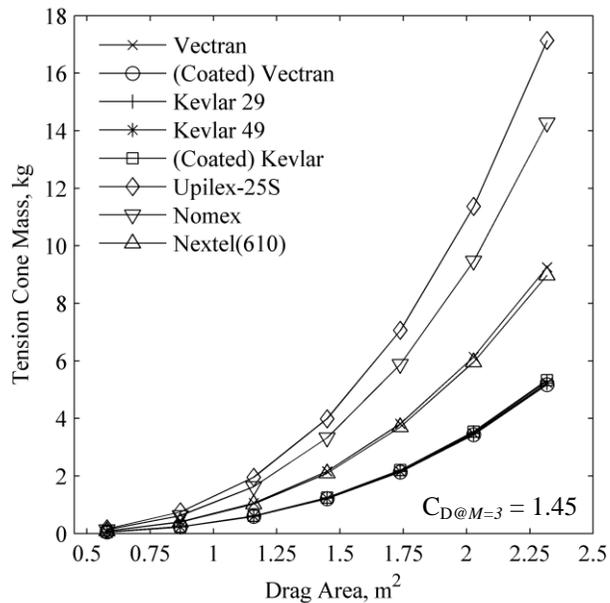

Figure 12. Decelerator mass as a function of drag area for a tension cone.

The estimated mass values are comparable to historical testing articles. The TD5840 test article consisted of a 1.5 m diameter attached isotensoid fabric mass was 1.9 kg deployed at a dynamic pressure of 5.75 kPa.[39] The TD

7

6929 attached isotensoid test article, also 1.5 m in diameter, had a mass of 0.98 kg tested up to dynamic pressures of 28 kPa.[40]
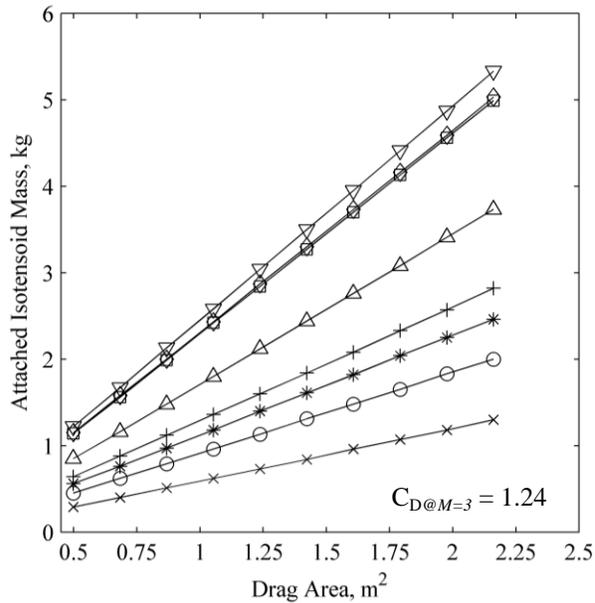

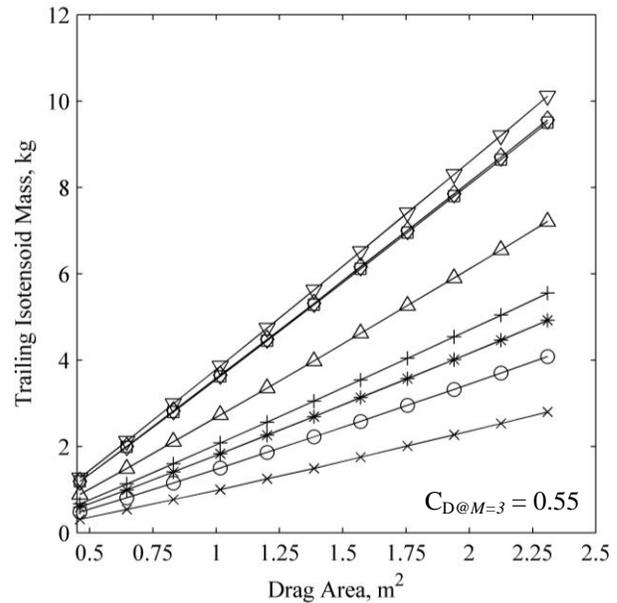**Figure 13. Decelerator mass as a function of drag area for an attached isotensoid**

Figure 14. Decelerator mass as a function of drag area for a trailing isotensoid

A priority vector, shown in Table V, was created by comparing the masses of each decelerator made of coated Vectran with a drag area of 1 m². This aerodynamic priority vector was implemented in the overall TOPSIS analysis for decelerator evaluation. The smaller number corresponds to the more favorable decelerator option, which was determined to be the attached isotensoid.

Table V. Mass AHP results

Decelerator Type	Priority Vector
Tension Cone	0.329
Attached Isotensoid	0.222
Trailing Isotensoid	0.449

C. Vehicle Integration

Vehicle integration metrics were divided into four decelerator mechanisms: attachment, storage, deployment and inflation. These mechanisms encompass the primary functional modes of the decelerator systems and must be incorporated into interface considerations with the vehicle bus. Table VI below provides a brief description of each mechanism for each decelerator.

Table VI. Decelerator integration mechanisms and descriptions.

Mechanism	Tension Cone	Attached Isotensoid	Trailing Isotensoid
Attachment			
Location	Leading edge	Leading edge	Rear edge
Interface	Single *tension hoop*	2 *tension hoops* (one for front surface and one for rear surface)	1 or more *bridle attachment points*
Storage			
Location	Front (external to bus structure)	Front (external to bus structure)	Rear (internal or external to bus structure)
Devices	*Braided corset* used to wrap decelerator and fasten to bus	*Braided corset* used to wrap decelerator and fasten to bus	Packaged similar to that of a small parachute
Deployment			
Devices	*Pyrotechnic cutters* used to sever corset lacing and inflation system begins to release pressurized gas	*Pyrotechnic cutters* used to sever corset lacing and *pre-inflation gas generator* releases pressurized gas	*Mortar gun* ejects small mass to pull decelerator out and *pre-inflation gas generator* releases pressurized gas
Inflation			
Devices	*Internal inflation system* provides pressurized gas to decelerator	*Ram-air inlets* guide freestream air into the decelerator	*Ram-air inlets* guide freestream air into the decelerator

8

The devices italicized in Table VI are devices needed for their respective mechanisms. A description of each these devices and supplemental resources are found below:

- *Tension hoops* are devices that secure the fabric of the decelerator to the metal bus structure via a clamping mechanism. The fabric material is clamped between metal plates which are reinforced with bolts.
- *Bridle attachment points* are the location where the decelerator is fastened to the bus structure usually with bolts.[19,36]
- *Braided corset* is a tie-down device made of flexible material that is held together with lacing.[41]
- *Pyrotechnic cutters* are devices that are capable of cutting cords using an explosive event.[42]
- *Internal inflation system* is a gas generation system located within the vehicle bus. This device can be a pressure vessel with inert gas stored at high pressures or a system which expels gas as a by-product of a chemical reaction.[43]
- *Pre-inflation gas system* is a gas generation system need to expose the ram-air inlets to the free stream. This is usually a small vial of methyl alcohol. The gas vaporized from this solution starts the inflation process for the isotensoid.[33]
- *Mortar gun* is a small launcher that deploys a small lumped mass to begin deployment process.[44]
- *Ram-air inlets* are devices that are located on the windward side of the decelerator and guide free stream air to the internal structure of the decelerator.[15,39]

The decelerator devices in a stowed configuration were examined using parachute packing densities. Without using pressurized packaging, the stowed decelerator packing density is estimated to be 320 kg/m^3.[36] For the coated Vectran material, storage volume as a function of drag area for the three decelerator types are shown in Figure 15. The attached isotensoid is the most storage efficient while the trailing isotensoid requires the greatest storage volume. Storage volume could also be improved if pressurized packaging was implemented.[45]
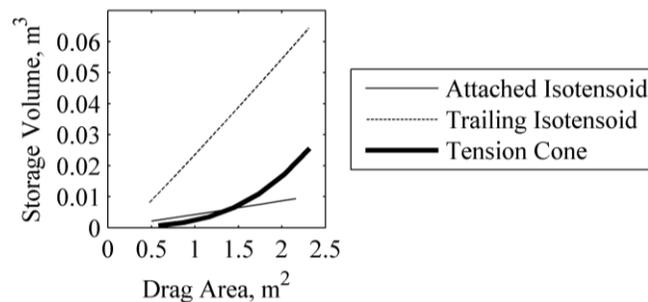

Figure 15. Decelerator storage volume as a function of decelerator drag area.

Based on the aforementioned vehicle integration considerations, pairwise priority vectors were created for each mechanism based on stakeholder input which were then summed together to generate to generate an overall vehicle integration weighting vector. As shown in Table VII, this integration priority vector was implemented in the overall TOPSIS analysis for decelerator evaluation. The values shaded in Table VII number corresponds to the more favorable options within each respective category.

The isotensoid decelerator, from a vehicle integration perspective, has a less complex inflation mechanism since an onboard inflation system is not required. The attachment mechanism vector favored the trailing isotensoid in particular due to the extensive flight testing that has demonstrated the reliability of that mechanism. The attached isotensoid required multiple attachment points, which increases overall complexity of that system. Again, the storage and deployments mechanisms favor the heritage hardware of the trailing isotensoid.

9

Table VII. Vehicle integration mechanism weighted priority vectors.

Decelerator	Tension Cone	Attached Isotensoid	Trailing Isotensoid
Attachment Mechanism	0.017	0.015	0.04
Storage Mechanism	0.047	0.047	0.142
Deployment Mechanism	0.091	0.091	0.272
Inflation Mechanism	0.026	0.106	0.106
Overall Weight Vector	**0.182**	**0.259**	**0.559**

D. Decelerator Evaluation

The priority weighting vectors for each integration mechanism were combined with an overall design metrics priority vector that were then used in a TOPSIS analysis. The design metrics priority vector, shown in Table VIII, was developed based on the stakeholders involved in this study, which identified aerodynamics and vehicle integration as the primary drivers in this evaluation. The results of the TOPSIS analysis are shown in Table IX. The trailing isotensoid is calculated to be the more ideal configuration given the aforementioned input priority vectors. However, the tension cone and the attached isotensoid are found to be comparable to the trailing isotensoid. The tension cone exhibits the overall greatest aerodynamic performance but its required inflation system is disadvantageous to its vehicle integration score. The attached isotensoid exhibits the second best aerodynamic performance but its required two attachment points also increase its vehicle integration complexity. With proven flight test articles, the trailing isotensoid exhibits marginal aerodynamic performance and proven vehicle integration mechanisms.

Table VIII. Design Metrics AHP results

Design Metric	Priority Vector
Mass	0.143
Aerodynamics	0.429
Vehicle Integration	0.429

Table IX. TOPSIS Euclidean distance to the ideal solution.

Decelerator Type	Relative Closeness to Ideal
Tension Cone	0.562
Attached Isotensoid	0.550
Trailing Isotensoid	0.446

V. Conclusion

The objective of this study was to evaluate three IAD configurations on a sounding rocket payload for atmospheric sample capture. A tension cone, attached isotensoid, and trailing isotensoid IAD were each investigated. Each IAD configuration was evaluated considering mass, aerodynamic performance, and vehicle integration. In terms of aerodynamic drag performance, the tension cone is the preferred choice for the sizes investigated. The attached isotensoid was shown to be the most mass efficient decelerator, while the trailing isotensoid was found to be the more ideal decelerator for vehicle integration. Heritage test vehicles have repeatedly proven the trailing isotensoid integration and deployment system. For the weightings considered in this mission concept, the trailing isotensoid was found to be the preferred configuration.

Acknowledgments

References

[1]H. Heidt, J. Puig-Suari, A. Moore, S. Nakasuka and R. Twiggs, "CubeSat: A new Generation of Picosatellite for Education and Industry Low-Cost Space Experimentation," in *AIAA/USU Conference on Small*

Satellites, 2000.

[2]*NASA Sounding Rocket Handbook,* Goddard Spaceflight Center: Wallops Flight Facility, 2006.

[3]M. Miller, B. Steinfeldt and R. and Braun, "Mission Architecture Considerations for Recovery of High-Altitude Atmospheric Dust Samples," in *AIAA Atmospheric Flight Mechanics Conference*, Boston, MA, 2013.

[4]R. Latteck and W. Singer, "Multi-Beam Radar Observations of Polar Mesosphere Summer Echoes During the MIDAS/DROPPS/MINIDUSTRY Campaign at Andenes, Norway," *Adv. Space Res,* vol. 28, pp. 1065-1070, 2001.

[5]C. Croskey, J. Mitchell and M. Friedrich, "Charged Particle Measurements in the Polar Summer Mesosphere Obtained by the DROPPS Sounding Rockets," *Adv. Space Res,* vol. 28, pp. 1047-1052, 2001.

[6]M. Rodríguez, *Analysis of the dynamical behavior of the Minidusty rocket payloads, and its influence on the plasma probe measurements,* Tromsø, Norway: MS Thesis. Department of Physics and Technology, University of Tromsø, 2007.

[7]S. Robertson, M. Horanyi and S. Knappmille, "Mass Analysis of Charged Aerosol Particles in NLC and PMSE during the ECOMA/MASS Campaign," *Annales Geophysicae,* vol. 27, 2009.

[8]B. Smith, C. Tanner, M. Mahzari, I. Clark, R. Braun and F. Cheatwood, "A Historical Review of Inflatable Aerodynamic Decelerator Technology Development," in *2010 IEEE Aerospace Conference*, Big Sky, MT, 2010.

[9]F. Nebiker, "Aerodynamic Deployable Decelerator Performance Evaluation Program, Phase I," AFFDL – TR67-27, 1965.

[10]F. Nebiker, "PEPP Ballute Design and Development Final Report," NASA – CR 66585, 1967.

[11]R. Braun and R. Manning, "Mars Exploration Entry, Descent, and Landing Challenges," *Journal of Spacecraft and Rockets,* vol. 44, no. 2, pp. 310-323, 2007.

[12]Z. Putnam and R. Braun, "Precision Landing at Mars Using Discrete-event Drag Modulation," in *23rd AAS/AIAA Spaceflight Mechanics Meeting*, Kauai, HI, 2013.

[13]L. Levy, "The Use of Drag Modulation to Limit the Rate at Which Deceleration Increases During Nonlifting Entry," NASA TN D-1037, Washington, DC, 1961.

[14]M. Burchell and e. al., "Characteristics of cometary dust tracks in Stardust Aerogel and laboratory calibrations," *Meteorite. Planet. Sci.,* vol. 43, pp. 23-40, 2008.

[15]C. Tanner, *Aeroelastic Analysis and Testing of Supersonic Inflatable Aerodynamic Decelerators,* Atlanta, GA: PhD Thesis. Department of Aerospace Engineering, Georgia Institute of Technology, 2012..

[16]I. Clark, *Aerodynamic Design, Analysis and Validation of a Supersonic Inflatable Decelerator,* Atlanta, GA: PhD Thesis. Department of Aerospace Engineering, Georgia Institute of Technology, 2009.

[17]I. Clark, A. Hutchings, C. Tanner and R. and Braun, "Supersonic Inflatable Aerodynamic Decelerators for Use on Future Robotic Missions to Mars," *Journal of Spacecraft and Rockets,* vol. 46, no. 2, pp. 340-352, 2009..

[18]R. Barton, "Development of Attached Inflatable Decelerators for Supersonic Application," NASA CR-66613, 1968..

[19]J. Usry, "Performance of a Towed, 48-inch-Diameter Ballute Decelerator Tested in Free Flight at Mach Numbers from 4.2 to 0.4," NASA TN D-4943, Hampton, Va, 1969.

[20]D. Kinney, "Aero-Thermodynamics for Conceptual Design," in *2004 AIAA Aerospace Sciences Meeting and Exhibit*, Reno, NV, 2004.

[21]"FUN3D Manual," NASA Langley, [Online]. Available: http://fun3d.larc.nasa.gov. [Accessed Oct 2009].

[22]W. Anderson and D. Bonhaus, "An Implicit Upwind Algorithm for Computing Turbulent Flows on Unstructured Grids," *Computers and Fluids,* vol. 23, pp. 1-22, 1994.

[23]J. P. Steinbrenner and J. Abelanet, "Anisotropic Tetrahedral Meshing Based on Surface Deformation Techniques," in *AIAA 45th Aerospace Sciences Meeting*, Reno, NV, 2007.

[24]J. Samareh, "Estimating Mass of Inflatable Aerodynamic Decelerators Using Dimensionless Parameters," in *8th International Planetary Probe Workshop*, Portsmouth, Virginia, 2011.

[25]M. S. Anderson, H. L. Bohon and M. M. and Mikulus, "A Structural Merit Function for Aerodynamic

Decelerators," NASA-TND-5535, 1969..

[26]J. Stein and C. Sandy, "Recent Developments in Inflatable Airbag Impact Attenuation Systems for Mars Exploration," in *AIAA Paper 2003-1900*, 2003.

[27]"Vetran Materials Datasheet," [Online]. Available: http://imattec.com/linked/vectran%20-%20technical%20data.pdf.

[28]"Kevlar Materials Datasheet," [Online]. Available: http://www2.dupont.com/Kevlar/en_US/assets/downloads/KEVLAR_Technical_Guide.pdf.

[29]R. Niccum, J. Munson and L. Rueter, "Investigation of Kevlar Fabric-Based Materials for Use with Inflatable Structures," NASA CR-2724, 1977.

[30]"Upilex Materials Datasheet," [Online]. Available: http://www.ube.com/content.php?pageid=81.

[31]"Nomex Materials Datasheet," [Online]. Available: http://www2.dupont.com/Personal_Protection/en_US/assets/downloads/nomex/Nomex_Technical_Guide.pdf.

[32]D. M. Wilson, "Statistical tensile strength of Nextel™ 610 and Nextel™ 720 fibers," 3M Metal Matrix Composites Department, St. Paul, Minnesota.

[33]F. Bloetscher, "Aerodynamic Deployable Decelerator Performance Evaluation Program, Phase II," AFFDL – TR67-25, 1967.

[34]T. Saaty, Multi criteria decision making: The analytic hierarchy process, New York: McGraw-Hill, 1980.

[35]J. Lafleur, "Probabilistic AHP and TOPSIS for Multi-Attribute Decision-Making under Uncertainty," in *2011 IEEE Aerospace Conference*, Big Sky, MT, 2011.

[36]T. Knacke, Parachute Recovery Systems: Design Manual, Santa Barbara, CA, 1992.

[37]C. Hwang and K. Yoon, "Multiple Attribute Decision Making," in *Springer-Verlag*, Berlin, 1981.

38K. Yoon, "Systems Selection by Multiple Attribute Decision Making," PhD Thesis, Department of Industrial Engineering, Kansas State University, 1980.

[39]H. Bohon and R. Miserentino, "Deployment and Performance Characteristics of 1.5m Attached Inflatable Decelerators from Mach 2.2 to 4.4," NASA TN D- 5840, NASA Langley Research Center, 1970.

[40]C. Willis and M. Mikulas, "Static Structural Tests of a 1.5-Meter-Diameter Fabric Attached Inflatable Decelerator," NASA Langley Research Center TN D-6929, Hampton, VA, 1972.

[41]D. Coatta and e. al., "Development and Testing of an 8 Meter Isotensoid Supersonic Inflatable Aerodynamic Decelerator," in *AIAA Aerodynamic Decelerator Systems (ADS) Conference*, Daytona Beach, Florida, 2013.

[42]Y. Chang, *Pyrotechnic Devices, Shock Levels And Their Applications,* Presented at Pyroshock Seminar, ICSV9, 2002.

[43]G. Brown, C. Epp, C. Graves, J. Lingard and M. Darly, *Hypercone Inflatable Supersonic Decelerator,* AIAA Paper 2003-2167, 2003.

[44]Sengupta, A., et al., "Overview of the Mars Science Laboratory Parachute Decelerator Subsystem," 2007

[45]M. Ivanov and e. al., ""Entry, Descent and Landing Systems Analysis Study: Phase 2 Report on Mars Science Laboratory Improvement," NASA/TM-2011-216988, 2011.